Scientific Research Publishing

Advances in Materials Physics and Chemistry, 2024, 14, 235-247
https://www.scirp.org/journal/ampc
ISSN Online: 2162-5328
ISSN Print: 2162-531X

Heat-Generating Effects Involving Multiple Nanofluids in a Hybrid Convective Boundary Layer Flow on the Sloping Plate in a Porous Medium

Md. Nasir Uddin*, Md. Abdullah Al Mamun, Md. Masudar Rahman

Department of Mathematics, Bangladesh Army University of Engineering & Technology, Natore, Bangladesh
Email: *mnasiruddin07@gmail.com

How to cite this paper: Uddin, Md.N., Al Mamun, Md.A. and Rahman, Md.M. (2024) Heat-Generating Effects Involving Multiple Nanofluids in a Hybrid Convective Boundary Layer Flow on the Sloping Plate in a Porous Medium. *Advances in Materials Physics and Chemistry*, **14**, 235-247.
https://doi.org/10.4236/ampc.2024.1410017

Received: September 10, 2024
Accepted: October 28, 2024
Published: October 31, 2024

Abstract

The hybrid convective boundary layer circulation involving multiple nanofluids via a medium with pores is approaching a sloping plate. An investigation regarding the heat-generating effects upon the examined nanofluid flows has been carried out through computational analysis. A mathematical framework employing governing differential equations that are partial has been implemented to produce an ensemble of ordinary differential equations, which happen to be nonlinear that incorporate nanofluid flows by utilizing acceptable transformations. Through the combination of the Nachtsheim-Swigert shooting method and the Runge-Kutta method, the group of resulting non-dimensionalized equations is solved computationally. In a few special, confined cases, the corresponding numeric output is thereafter satisfactorily matched with the existing available research. The consequences of heat generation regarding local skin friction coefficient and rate of heat in conjunction with mass transfer have been investigated, evaluated, and reported on the basis of multiple nanofluid flows.

Keywords

Heat-Generating, Hybrid Convection, Nanofluids, Porous Medium, Sloping Plate

1. Introduction

There are numerous real-world applications regarding the study of heat transport as well as fluid flow, including drying porous materials, pharmaceutical processes, geophysical systems, glassmaking, thermal insulation, oil recovery, hybrid-powered

engines, and solar thermal systems. The rate of convective heat and mass transfer as well as corresponding coefficients for shear rate impact the overall performance of the finished good, making the key industrial applications of heat and mass transfer in conjunction with flow analysis significant. With their increased thermophysical features and heat-together mass transfer appearance, nanofluids have the capability to be heat-transfer fluids with enhanced efficiency for a variety of purposes. The transformation of complex forms into linear forms has attracted the attention of numerous academics because of its wide range of important physical applications.

The influence of heat creation/absorption during a thermally radiative blended convective circulation of the zinc (Zn)—titanium dioxide/water (TiO_2/H_2O) nanofluid mixtures over a sloped, shrinking surface has been addressed via Yasir *et al*. [1]. They covered the consequences of controlling characteristics on skin friction coefficient with regard to the velocity and local Nusselt number with regard to the temperature. The study carried out by Rana *et al*. [2] examined the steady mixed convection boundary layer movement that occurred in an incompressible nanofluid in a porous environment along a plate sloped at an angle of α. They thoroughly explored the impacts of the combined convection parameter, buoyancy ratio, and Lewis number upon temperature, along with concentration distributions. According to Uddin *et al*. [3], combined convection of flow of nanofluid, including viscous dissipation throughout the surrounding porous environment, has been addressed and observed the impact of Schmidt number, permeability of porous medium, and Eckert number. Zainodin *et al*. [4] have examined how an inclination angle affects mixed convection hybrid ferrofluid flow on a porous shrink surface, taking into account convective boundary conditions and heat sources.

The impact of thermal radiation, along with convection and conduction, upon an unstable boundary layer of heat transfer and flow of nanofluid throughout a permeable, moveable surface through a medium with pores has been addressed by Sedik *et al*. [5]. They have additionally discussed the consequences of heat generation. Aznam *et al*. [6] have examined the impact for magnetic strength regarding magnetohydrodynamic (MHD)-free convection flow of nanofluids with Newtonian heating through a sliding inclined plate. Both an analytical and numerical, tabular evaluations of the skin friction and Nusselt number have been conducted. Graphical representations of the velocity and temperature numerical findings have been provided for a range of relevant factors. Cimpean and Pop [7] have reported the completely developed nanofluid with mixed convection circulation in a channel filled with a material with pores that remains steady. For three distinct nanofluids, the consequences of these factors on the fluid's flow as well as heat transport features, have been thoroughly examined. In a porous environment having viscous dissipation, Uddin *et al*. [8] have studied the double-diffusive transfer regarding mass and heat features involving hybrid convective copper-water nanofluid flow via a sloped plate with the existence like as a field of magnetic

particles.

According to Khan *et al*. [9], the fluid that is not Newtonian is affected by homogeneous fluid suction, and the unstable flow over a vertically extended porous plate is impacted by radiation from heat as well as chemical processes. They have found that the temperature profile is higher while comparing with the parameter of heat source and lower in relation to the heat sink parameter over the whole boundary layer. A dependent on temperature source of heat or sink and the finding that the mean Nusselt number decreases with different nanofluids are among the consequences of the improvement in heat transfer associated with boundary layer flow, which has been studied via Rana and Bhargava [10] under conditions of steady state and involves several forms of nanofluid flows moving on a vertical plate. Moreover, Abbasi *et al*. [11] reported on the dual layered combined convective magneto-hydrodynamic flow on the basis of other than Newtonian nanofluid presence involving Brownian processes, thermophoresis, and heat absorption/generation. The computational findings have been displayed and assessed. Through the work of Upreti *et al*. [12], the flow characteristics of MHD concerning the nanofluid through a pores flat plate along with viscous-Ohmic dissipation, heat generation/absorption, and injection/suction has been investigated. Even if the contrary tendency is observed when taking into account the thermal boundary layer, the researchers illustrated aspects like how the value of thickness with regard to the momentum boundary layer decays together in order with the advancing values depending on the segment of volume due to a fact that silver particles are solid.

In terms of several nanofluids on hybrid convection in porous medium for a sloping plate together with the current physical properties, no studies have, according to what the authors came to know, been published. In order to fill what is missing in the existing literature, the aim of the up-to-date investigation is to explore how to develop mass and heat transfer along with steady boundary layer flow in homogenous porous medium that is saturated with nanofluids in the scenario of a sloping plate in conjunction with heat generation and chemical reaction effect.

2. Problem Assumptions with Mathematical Formulation

Water is considered to act as the basic fluid in a hybrid convective flow of the boundary layer across a sloping plate in a medium with holes. The heat-generating consequences for multiple nanofluids are currently being investigated. Furthermore, there is a localized temperature balance involving the base fluid and the particles that adopt nanoparticles. **Figure 1**, which is a relationship, shows a visual representation of the flow model including the arrangement of coordinates for the investigation field.

The direction of flow is indicated by the x-axis of measurement, which flows parallel to the plate, and the flow direction is indicated by the y-axis, which flows at right angles to the plate. The velocity elements in both directions of movement

are also represented by variables with names u and v, accordingly. A sloping plate with a slope of α is parallel to the flow field's consistent external velocity U_∞. Acceleration-induced gravitation is symbolized by the character g. T and C are the temperature and concentration of the fluid flow in the boundary layer, however the plate's wall has greater values of T_w and C_w, compared to the ambient circumstances, T_∞ and C_∞, respectively.

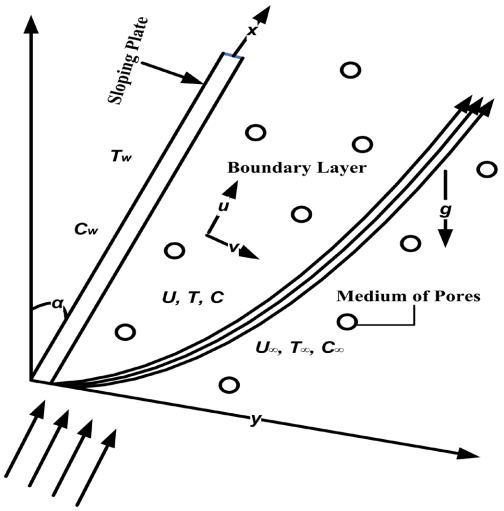

Figure 1. Visual representation for the flow model including coordinate system.

The subsequent equations, which make use of the previously mentioned characteristics, are employed to discuss consistent, two-dimensional in nature laminar boundary-layer flow:

$$\frac{\partial u}{\partial x}+\frac{\partial v}{\partial y}=0 \tag{1}$$

$$\begin{aligned} u\frac{\partial u}{\partial x}+v\frac{\partial u}{\partial y}&=\nu_{nf}\left\{\frac{\partial^2 u}{\partial y^2}-\frac{1}{k_{pp}}\left(u-U_\infty\right)\right\}\\ &+\frac{g}{\rho_{nf}}\left\{\left(\rho\beta_t\right)_{nf}\left(T-T_\infty\right)+\left(\rho\beta_c\right)_{nf}\left(C-C_\infty\right)\right\}\cos\alpha \end{aligned} \tag{2}$$

$$u\frac{\partial T}{\partial x}+v\frac{\partial T}{\partial y}=\alpha_{nf}\frac{\partial^2 T}{\partial y^2}+\frac{\mu_{nf}}{\left(\rho C_p\right)_{nf}}\left\{\frac{Q_0}{\mu_{nf}}\left(T-T_\infty\right)+u\frac{\partial^2 u}{\partial y^2}+\left(\frac{\partial u}{\partial y}\right)^2\right\} \tag{3}$$

$$u\frac{\partial C}{\partial x}+v\frac{\partial C}{\partial y}=D\frac{\partial^2 C}{\partial y^2}-k_{rp}\left(C-C_\infty\right) \tag{4}$$

The parameters μ_{nf}, ν_{nf}, ρ_{nf}, $(\beta_c)_{nf}$ and $(\beta_t)_{nf}$ reveal the dynamic viscosity, kinematic viscosity, density, coefficient of expansion due to concentration and temperature of the nanofluid, respectively whereas $(\rho C_p)_{nf}$ and α_{nf} expose the heat capacitance and thermal diffusivity of the nanofluid, correspondingly. Moreover, k_{pp}, Q_0, k_{rp} and D disclose the permeability of the porous medium, heat generation

constant, chemical reaction and mass diffusivity of the flow, individually. Reviewing the articles of Bachok *et al.* [13] and Pal and Mandal [14] will help to develop an extensive knowledge of the governing equations.

The subsequent relationships regarding the physical characteristics of the base fluid and nanoparticle have been demonstrated by Brinkman [15] and Abu-Nada [16]:

$$\mu_{nf}=\frac{\mu_{bf}}{(1-\phi)^{2.5}},\frac{K_{nf}}{K_{bf}}=\frac{(2K_{bf}+K_{np})-2\phi(K_{bf}-K_{np})}{(2K_{bf}+K_{np})+\phi(K_{bf}-K_{np})},\nu_{nf}=\frac{\mu_{nf}}{\rho_{nf}},$$

$$\rho_{nf}=\phi\rho_{np}+(1-\phi)\rho_{bf},(\rho\beta_t)_{nf}=\phi(\rho\beta_t)_{np}+(1-\phi)(\rho\beta_t)_{bf},\alpha_{nf}=\frac{K_{nf}}{(\rho C_p)_{nf}}, \quad (5)$$

$$(\rho\beta_c)_{nf}=\phi(\rho\beta_c)_{np}+(1-\phi)(\rho\beta_c)_{bf} \text{ and } (\rho C_p)_{nf}=\phi(\rho C_p)_{np}+(1-\phi)(\rho C_p)_{bf}$$

In which the subscripts *nf* and *np* indicate for a nanofluid and nanoparticle, accordingly, and the subscripts *bf* a water-like base fluid and ϕ indicates the nanoparticle solid volume fraction. With respect to the present nanofluid flow field, the appropriate boundaries are considered:

$$u=0,\ v=0,\ T=T_w \text{ and } C=C_w \quad \text{at } y=0 \quad (6)$$

$$u\to U_\infty,\ T\to T_\infty \text{ and } C\to C_\infty \quad \text{as } y\to\infty \quad (7)$$

where ∞ and *w* indicate the boundary layer and wall ends, correspondingly. The analysis is made easier by incorporating the dimensionless components that were created by Cebeci *et al.* [17], which results in the nondimensionality of the differential equations governing the analysis after the necessary transformations:

$$\eta=y\sqrt{\frac{U_\infty}{\nu_{bf}x}},\ \psi=\sqrt{\nu_{bf}xU_\infty}f(\eta),\ \theta(\eta)=\frac{T-T_\infty}{T_w-T_\infty} \text{ and } s(\eta)=\frac{C-C_\infty}{C_w-C_\infty} \quad (8)$$

Using the stream function, the velocity components can be formulated as follows:

$$\begin{aligned} &u=U_\infty f'(\eta) \text{ where } u=\frac{\partial\psi}{\partial y} \text{ and}\\ &v=\frac{1}{2}\sqrt{\frac{\nu_{bf}U_\infty}{x}}\left[\eta f'(\eta)-f(\eta)\right] \text{ where } v=-\frac{\partial\psi}{\partial x} \end{aligned} \quad (9)$$

as long as the prime reflects a differentiation with respect to η.

Dimensionless variables can be used to incorporate corresponding modified equations for momentum, energy, and concentration as well as accompanying boundary circumstances:

$$f'''+\frac{1}{2}\phi_1\phi_2 ff''+K(1-f')+\phi_1\{\phi_3 Ri_t\theta+\phi_4 Ri_c s\}\cos\alpha=0 \quad (10)$$

$$\theta''+\frac{1}{2}\Pr\left(\frac{\phi_6}{\phi_5}\right)f\theta'+\Pr Q\theta+\frac{\Pr Ec}{\phi_1\phi_5}\left(f'f'''+f''^2\right)=0 \quad (11)$$

$$s''+\frac{1}{2}Scfs'-ScK_{rp}s=0 \quad (12)$$

and under the boundary circumstances:

$$f=0,\ f'=0,\ \theta=1 \text{ and } s=1 \text{ at } \eta=0 \tag{13}$$

$$f'\to 1,\ \theta\to 0 \text{ and } s\to 0 \text{ as } \eta\to\infty \tag{14}$$

The following is a description of the physical parameters found in the dimensionless Equations (10)-(12):

$$\begin{aligned}
&Gr_c=\frac{x^3 g\left(C_w-C_\infty\right)\left(\beta_c\right)_{bf}}{\nu_{bf}^2}, Gr_t=\frac{x^3 g\left(T_w-T_\infty\right)\left(\beta_t\right)_{bf}}{\nu_{bf}^2}, Ri_c=\frac{Gr_c}{\left(\mathrm{Re}_x\right)^2},\\
&Ri_t=\frac{Gr_t}{\left(\mathrm{Re}_x\right)^2}, \mathrm{Re}_x=\frac{xU_\infty}{\nu_{bf}}, \mathrm{Pr}=\frac{\left(\rho C_p\right)_{bf}\nu_{bf}}{K_{bf}}, K=\frac{x\nu_{bf}}{k_{pp}U_\infty},\\
&Q=\frac{xQ_0}{\left(\rho C_p\right)_{bf}U_\infty}, Ec=\frac{U_\infty^2}{\left(C_p\right)_{bf}\left(T_w-T_\infty\right)}, Sc=\frac{\nu_{bf}}{D}, K_{rp}=\frac{xk_{rp}}{U_\infty},\\
&\phi_1=\left(1-\phi\right)^{2.5}, \phi_2=\phi\frac{\rho_{np}}{\rho_{bf}}+\left(1-\phi\right), \phi_3=\phi\frac{\left(\rho\beta_t\right)_{np}}{\left(\rho\beta_t\right)_{bf}}+\left(1-\phi\right),\\
&\phi_4=\phi\frac{\left(\rho\beta_c\right)_{np}}{\left(\rho\beta_c\right)_{bf}}+\left(1-\phi\right), \phi_5=\frac{K_{nf}}{K_{bf}} \text{ and } \phi_6=\phi\frac{\left(\rho C_p\right)_{np}}{\left(\rho C_p\right)_{bf}}+\left(1-\phi\right)
\end{aligned} \tag{15}$$

The parameters Re_x, Ri_c, and Ri_t reveal the local Reynolds number, the local Richardson number for mass, and the local Richardson number for thermal, respectively, whereas Gr_c and Gr_t reveal the local Grashof number for mass and the local Grashof number for thermal, correspondingly. Moreover, the parameters Sc, K_{rp}, K, Q, Ec and Pr expose the Schmidt number, the chemical reaction parameter, the permeability parameter, the heat generation parameter, the Eckert number and the Prandtl number, whereas $\phi_i\left(i=1,2,\cdots,6\right)$ exposes constants, respectively. According to Ahmed *et al.* [18], the characteristics of the base fluid and nanoparticles are displayed in **Table 1** from a thermophysical aspect for nanofluid flow.

Table 1. Properties of base fluid and nanoparticles from a thermophysical perspective for fluid flow.

Attributes	Thermophysical Perspective				
	σ (S/m)	β (1/K)	ρ (kg/m^3)	k (W/m·K)	C_p (J/kg·K)
Water (H_2O)	0.05	21×10^{-5}	997.1	0.613	4179
Aluminium Oxide (Al_2O_3)	1×10^{-10}	0.85×10^{-5}	3970	40	765
Copper (Cu)	5.96×10^{7}	1.67×10^{-5}	8933	401	385
Silver (Ag)	3.6×10^{7}	1.89×10^{-5}	10500	429	235

It is feasible to ascertain the nondimensional types of $C_f=\frac{2}{\phi_1}\left(\mathrm{Re}_x\right)^{-\frac{1}{2}}f''\left(0\right)$

as local skin-friction coefficient, $Nu_x = -\phi_5 \left(\mathrm{Re}_x\right)^{\frac{1}{2}} \theta'(0)$ as local Nusselt number, and $Sh = -\left(\mathrm{Re}_x\right)^{\frac{1}{2}} s'(0)$ as local Sherwood number by applying the wall shear stress definition in conjunction with Fourier's law and Fick's law.

3. Numerical Approaches for Solving

After employing the FORTRAN programming coding to locate the unknown beginning circumstances of dimensionless momentum, energy, and concentration equations, Nachtsheim and Swigert [19] established a strategy to deal with the system with respect to of the acquired boundary value problem, e.g., Equations. (10)-(12), together with in combination of the corresponding boundary circumstances, such as Equations (13)-(14). Once the unknown starting constraints are identified, the newly generated boundary value system is re-transformed, becoming a problem with initial values on its way to the initial value system. The thereby produced system is computationally addressed utilising sixth-order Runge-Kutta strategies. In addition, the sixth-order Runge-Kutta strategies of Al-Shimmary [20] along with the useful computational methods of Nachtsheim and Swigert [19] are both taken into consideration.

4. Validation of the Model

With the utilization of copper (Cu)-water (H_2O) nanofluid, a comparison of the numerical value $f''(0)$ is performed adopting various values according to the ratio of velocity parameter λ, the volume fraction of nanoparticle ϕ, and the Prandtl number Pr by **Table 2**. For the sake of this work, the numerical strategy with reference to Nachtsheim and Swigert [19] has been developed as a result of the comparison's satisfying results. Furthermore, the numerical results derived from the current work will be discussed and presented in the next part.

Table 2. Comparison employing nanofluid of copper (Cu)-water (H_2O) with Pr = 6.2 with respect to the numerical values obtained from $f''(0)$ as well as various assumptions of ϕ and λ.

ϕ	λ	Blasius [21]	Ishak *et al.* [22]'s first solution	Bachok *et al.* [13]'s first solution	Present outcome as verified of Bachok *et al.*'s first solution [13]
0	−0.4	0.332	0.4357	0.4357	0.4366
	−0.2		0.4124	0.4124	0.4132
	0		0.3321	0.3321	0.3328
0.1	−0.4			0.5117	0.5128
	−0.2			0.4844	0.4853
	0			0.3901	0.3909
0.2	−0.4			0.5306	0.5316
	−0.2			0.5023	0.5031
	0			0.4045	0.4052

5. Findings and Discussion

For the purpose of demonstrating the impacts of the heat-generating parameter Q, detailed numerical results are worked out in relation to the flow of nanofluids of silver (Ag)-water (H_2O), as well as copper (Cu)-water (H_2O) and aluminum oxide (Al_2O_3)-water (H_2O). These results are obtained using various values for nondimensional parameters. The consequences upon the heat-generating factor for silver (Ag)-water (H_2O) nanofluid in conjunction with multiple types of nanofluids are illustrated graphically during the purposes of the flow fields' velocity is related to the local skin friction coefficient C_f, temperature is related to the local Nusselt number Nu_x, and concentration is related to the local Sherwood number Sh. Unless otherwise noted, the values for the silver (Ag)-water (H_2O) nanofluid take into account nondimensional parameters such $Ec = 0.1$, $\phi = 0.1$, Pr = 6.2, $Ri_c = 1$, $Ri_t = 1$, $U_\infty/\nu = 1.0$, $K = 0.5$, $\alpha = 30^\circ$, $K_{rp} = 0.5$, and $Sc = 0.22$. Nonetheless, the values that take into account nondimensional factors like Pr = 6.2, $\phi = 0.01$, $Q = 0.5$, $Ec = 0.1$, $Ri_c = 1$, $Ri_t = 1$, $U_\infty/\nu = 1.0$, $K = 0.1$, $K_{rp} = 0.5$, $\alpha = 30^\circ$, and $Sc = 0.22$, are thought to demonstrate the effects of various nanofluid kinds.

The flow parameters on the silver (Ag)-water (H_2O) nanofluid flow field, which include the heat-generating parameter Q corresponds to 0, 0.1, and 0.2, differ with respect to the velocity, temperature, and concentration in addition to the local skin friction, local Nusselt number, and local Sherwood number, as demonstrated through **Figures 2(a)-2(f)**. The rest of the parameters remain the same as well. **Figure 2(a)** illustrates how the buoyancy force increases with the generation

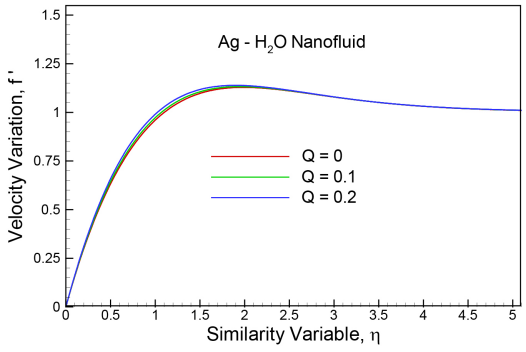

(a)

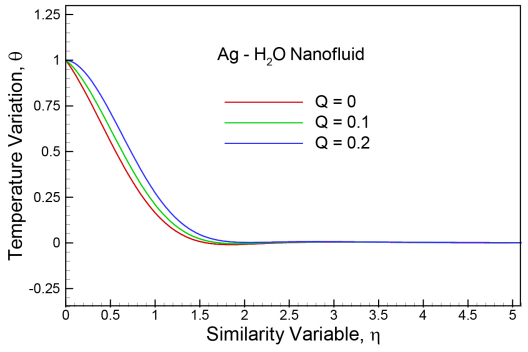

(b)

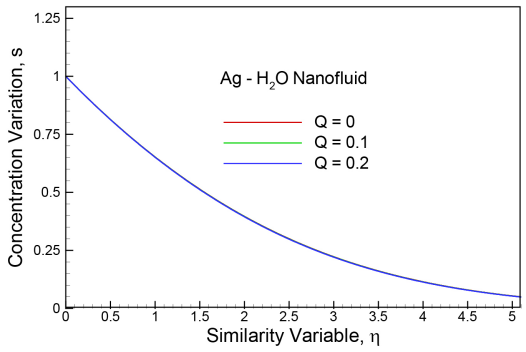

(c)

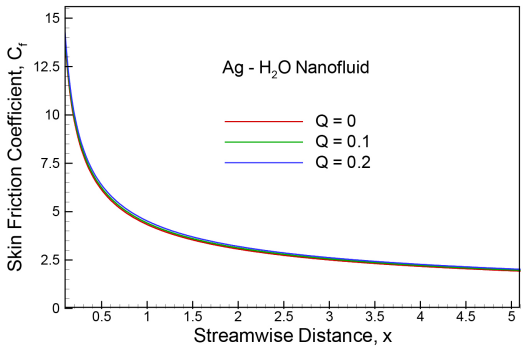

(d)

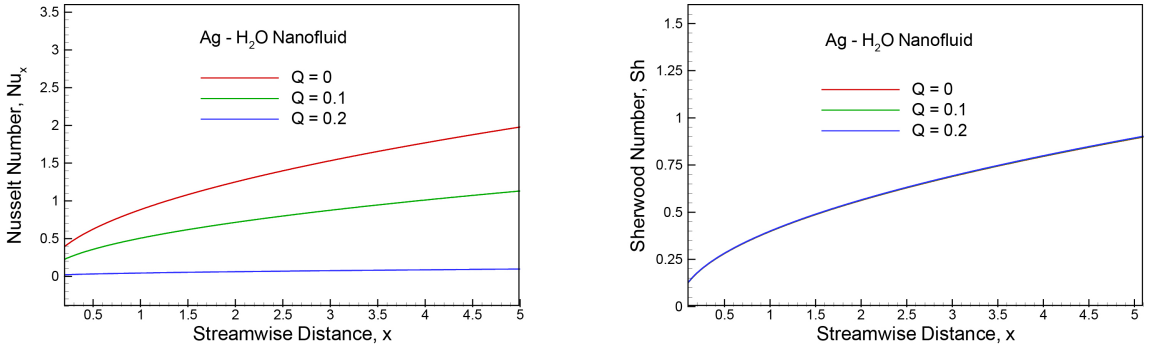

(e) (f)

Figure 2. (a) Velocity deviation affected by the parameter for heat generation Q; (b). Temperature deviation affected by the parameter for heat generation Q; (c) Concentration deviation affected by the parameter for heat generation Q; (d) Skin friction coefficient C_f deviation affected by the parameter for heat generation Q; (e) Local Nusselt number Nu_x deviation affected by the parameter for heat generation Q; (f) Local Sherwood number Sh deviation affected by the parameter for heat generation Q.

of heat, increasing the flow rate and the flow field's velocity as well, ultimately converging to the boundary condition. Furthermore, when the heat-generating parameter value grows, so does the thickness of the velocity boundary layer. The temperature of the fluid rises when a source of heating is present upon the flow field, which causes the thermal boundary layer to rise and eventually converge to the boundary condition. For this reason, it is observed in **Figure 2(b)** that when the value associated with the heat-generating parameter increases, so does the temperature distribution. The maximum fluid temperature occurs in the fluid region near the plate's surface rather than at the plate's surface when the heat source's strength is relatively high. A negligible change in the concentration distribution is observed when the value associated with the heat-generating parameter increases, as **Figure 2(c)** illustrates. **Figures 2(d)-2(f)** illustrate how the heat-generating parameter influences within the boundary layer in relation to the streamwise distance x for the local skin friction coefficient, local Nusselt number, and local Sherwood number. It is found that a rise in the heat generation parameter value causes the local coefficient of skin friction to increase and the local Nusselt number to drop; there is very little change in the local Sherwood number.

The impact of multiple kinds of nanofluids upon boundary layer flow patterns once velocity, together with temperature and concentration, are demonstrated with the assistance of **Figures 3(a)-3(c)**. Among the several types of nanofluids are aluminum oxide (Al_2O_3)-water (H_2O), silver (Ag)-water (H_2O) and copper (Cu)-water (H_2O). **Figure 3(a)** shows the velocity of the nanofluid flow such as aluminum oxide (Al_2O_3)-water (H_2O) to be higher than that of the copper (Cu)-water (H_2O) and silver (Ag)-water (H_2O) nanofluid flow and the boundary condition is then converged. Nevertheless, as it is observed in **Figure 3(b)**, the temperature of the nanofluid flow such as aluminum oxide (Al_2O_3)-water (H_2O) is differ insignificantly than that of the copper (Cu)-water (H_2O) and silver (Ag)-water (H_2O) as well as finally approaches the boundary condition. Furthermore,

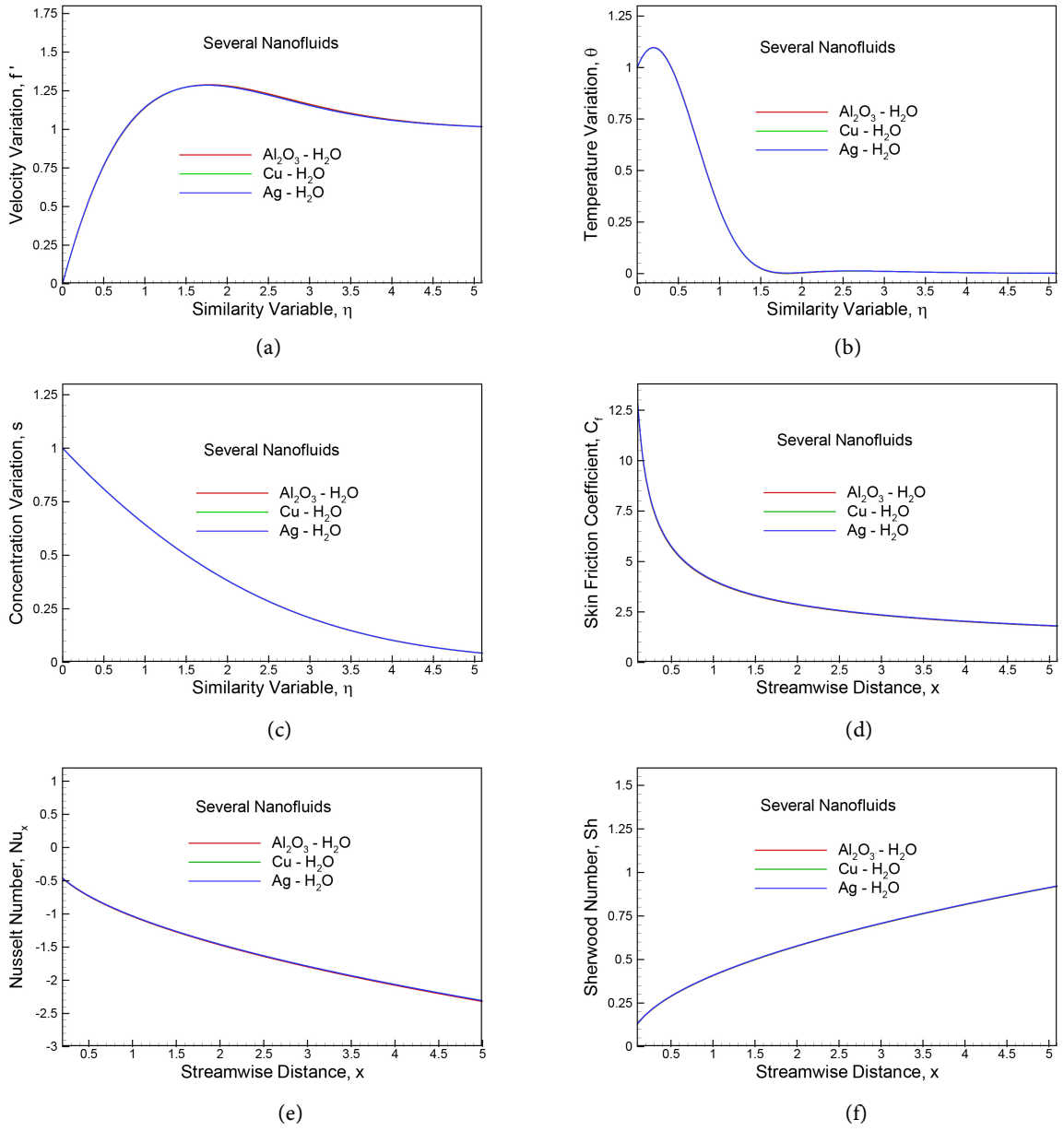

Figure 3. (a) Velocity deviation affected by the multiple types of nanofluids; (b) Temperature deviation affected by the multiple types of nanofluids; (c) Concentration deviation affected by the multiple types of nanofluids; (d). Skin friction coefficient C_f deviation affected by the multiple types of nanofluids; (e) Local Nusselt number Nu_x deviation affected by the multiple types of nanofluids; (f). Local Sherwood number Sh deviation affected by the multiple types of nanofluids.

it is shown through Figure 3(c) for concentration, the behavior of the nanofluid flows involving aluminum oxide (Al_2O_3)-water (H_2O), copper (Cu)-water (H_2O), and silver (Ag)-water (H_2O) is negligible. As a result, compared to aluminum oxide (Al_2O_3)-water (H_2O) and copper (Cu)-water (H_2O), the local skin friction coefficient C_f and the local Nusselt number Nu_x increase slightly due to silver (Ag)-water (H_2O) nanofluid flow, while the local Sherwood number Sh changes negligibly, as shown in Figures 3(d)-3(f).

In addition, for $\eta = 0$, the computational data of $f''(0)$ as well as $\theta'(0)$ and $s'(0)$ are exposed in Table 3 for silver (Ag)-water (H_2O) as well as Table 4 for multiple types of nanofluids.

Table 3. The computational data for $f''(0)$ as well as $\theta'(0)$ and $s'(0)$ in regard to $\eta = 0$, $\alpha = 30^\circ$, $Ri_c = 1.0$, $Ri_t = 1.0$, Pr = 6.2, $Sc = 0.22$, $K = 0.5$, $K_{rp} = 0.5$ and $Ec = 0.1$ for silver (Ag)-water (H_2O) nanofluid.

Features			$f''(0)$	$\theta'(0)$	$s'(0)$
Q	0	$\phi = 0.01$	1.83817522	−0.75111642	−0.40143595
	0.1		1.86128418	−0.50761644	−0.40185819
	0.2		1.89000728	−0.22846400	−0.40239724
Q	0	$\phi = 0.10$	1.66499662	−0.66400345	−0.39776447
	0.1		1.69195411	−0.37893610	−0.39830626
	0.2		1.72865167	−0.03136652	−0.39906876

Table 4. The computational data for $f''(0)$ as well as $\theta'(0)$ and $s'(0)$ in regard to $\eta = 0$, $\phi = 0.01$, $\alpha = 30^\circ$, $Q = 0.5$, $Ri_c = 1.0$, $Ri_t = 1.0$, Pr = 6.2, $Sc = 0.22$, $K = 0.1$, $K_{rp} = 0.5$ and $Ec = 0.1$ for multiple types nanofluids.

Features	$f''(0)$	$\theta'(0)$	$s'(0)$
Al_2O_3 - H_2O	1.96787627	1.00914179	−0.40716922
Cu - H_2O	1.97478183	1.00398009	−0.40714933
Ag - H_2O	1.97848544	1.00549783	−0.40717846

6. Conclusion

A computational investigation of the heat-generating consequences on the hybrid convective nanofluid of silver (Ag)-water (H_2O), copper (Cu)-water (H_2O), and aluminum oxide (Al_2O_3)-water (H_2O) flows along a sloping plate via the porous medium is carried out for the purposes of a recent study with respect to viscous dissipation and chemical reactions. For silver (Ag)-water (H_2O) nanofluid flow, raising the heat generation parameter values causes the flow field's temperature and velocity to rise, which reduces the local Nusselt number but raises the local skin friction coefficient. On the other hand, there is minimal variation in the concentration as well as the local Sherwood number. The aluminum oxide (Al_2O_3)-water (H_2O) nanofluid flow is shown to have a higher velocity than the nanofluid flows of copper (Cu)-water (H_2O) and silver (Ag)-water (H_2O), and the boundary condition is subsequently convergent. Although the concentration change is minimal, the temperature of the nanofluid flow such as aluminum oxide (Al_2O_3)-water (H_2O) is a little higher than it is for the copper (Cu)-water (H_2O) and silver (Ag)-water (H_2O) nanofluid flows. After that, the flows converge to the boundary condition. As a result, compared to aluminum oxide (Al_2O_3)-water (H_2O) and copper (Cu)-water (H_2O) nanofluid flows, the local skin friction coefficient C_f and the local Nusselt number Nu_x slightly increase due to silver (Ag)-water (H_2O)

nanofluid flow, while the local Sherwood number *Sh* varies negligibly. The findings of this study, along with information from physics, will be useful to the engineering and built-up segments, researchers, experimentalists, and recreation experts to better understand how heat generation and nanofluid flow function in intricate geometries.

Conflicts of Interest

The authors declare no conflicts of interest regarding the publication of this paper.

References

[1] Yasir, M., Khan, M., Alqahtani, A.S. and Malik, M.Y. (2023) Heat Generation/Absorption Effects in Thermally Radiative Mixed Convective flow of Zn-TiO_2/H_2O Hybrid Nanofluid. *Case Studies in Thermal Engineering*, **45**, Article ID: 103000.

[2] Rana, P., Bhargava, R. and Bég, O.A. (2012) Numerical Solution for Mixed Convection Boundary Layer Flow of a Nanofluid along an Inclined Plate Embedded in a Porous Medium. *Computers & Mathematics with Applications*, **64**, 2816-2832. https://doi.org/10.1016/j.camwa.2012.04.014

[3] Uddin, M.N., Alim, M.A. and Ahmed, S.R. (2019) Mixed Convective Nanofluid Flow with Viscous Dissipation in Surrounding Porous Medium. *American Journal of Engineering Research*, **8**, 299-306.

[4] Zainodin, S., Jamaludin, A., Nazar, R. and Pop, I. (2024) Impact of Heat Source on Mixed Convection Hybrid Ferrofluid Flow across a Shrinking Inclined Plate Subject to Convective Boundary Conditions. *Alexandria Engineering Journal*, **87**, 662-681. https://doi.org/10.1016/j.aej.2023.12.057

[5] Sedki, A.M., Abo-Dahab, S.M., Bouslimi, J. and Mahmoud, K.H. (2021) Thermal Radiation Effect on Unsteady Mixed Convection Boundary Layer Flow and Heat Transfer of Nanofluid over Permeable Stretching Surface through Porous Medium in the Presence of Heat Generation. *Science Progress*, **104**, page. https://doi.org/10.1177/00368504211042261

[6] Aznam, N.H.Z., Bosli, F., Ilias, M.R., Ishak, S.S., Ahmad, A.M. and Nayan, A. (2024) The Newtonian Heating Effect on MHD Free Convective Boundary Layer Flow of Magnetic Nanofluids Past a Moving Inclined Plate. *International Journal of Advanced and Applied Sciences*, **11**, 68-77.

[7] Cimpean, D.S. and Pop, I. (2012) Fully Developed Mixed Convection Flow of a Nanofluid through an Inclined Channel Filled with a Porous Medium. *International Journal of Heat and Mass Transfer*, **55**, 907-914. https://doi.org/10.1016/j.ijheatmasstransfer.2011.10.018

[8] Uddin, M.N., Alim, M.A. and Rahman, M.M. (2019) MHD Effects on Mixed Convective Nanofluid Flow with Viscous Dissipation in Surrounding Porous Medium. *Journal of Applied Mathematics and Physics*, **7**, 968-982. https://doi.org/10.4236/jamp.2019.74065

[9] Khan, Z., Khan, I., Ullah, M. and Tlili, I. (2018) Effect of Thermal Radiation and Chemical Reaction on Non-Newtonian Fluid through a Vertically Stretching Porous Plate with Uniform Suction. *Results in Physics*, **9**, 1086-1095. https://doi.org/10.1016/j.rinp.2018.03.041

[10] Rana, P. and Bhargava, R. (2011) Numerical Study of Heat Transfer Enhancement in Mixed Convection Flow along a Vertical Plate with Heat Source/Sink Utilizing Nanofluids. *Communications in Nonlinear Science and Numerical Simulation*, **16**, 4318-4334. https://doi.org/10.1016/j.cnsns.2011.03.014

[11] Abbasi, F.M., Shehzad, S.A., Hayat, T. and Ahmad, B. (2016) Doubly Stratified Mixed

Convection Flow of Maxwell Nanofluid with Heat Generation/Absorption. *Journal of Magnetism and Magnetic Materials*, **404**, 159-165. https://doi.org/10.1016/j.jmmm.2015.11.090

[12] Upreti, H., Pandey, A.K. and Kumar, M. (2018) MHD Flow of Ag-Water Nanofluid over a Flat Porous Plate with Viscous-Ohmic Dissipation, Suction/Injection and Heat Generation/Absorption. *Alexandria Engineering Journal*, **57**, 1839-1847. https://doi.org/10.1016/j.aej.2017.03.018

[13] Bachok, N., Ishak, A. and Pop, I. (2012) Flow and Heat Transfer Characteristics on a Moving Plate in a Nanofluid. *International Journal of Heat and Mass Transfer*, **55**, 642-648. https://doi.org/10.1016/j.ijheatmasstransfer.2011.10.047

[14] Pal, D. and Mandal, G. (2014) Influence of Thermal Radiation on Mixed Convection Heat and Mass Transfer Stagnation-Point Flow in Nanofluids over Stretching/shrinking Sheet in a Porous Medium with Chemical Reaction. *Nuclear Engineering and Design*, **273**, 644-652. https://doi.org/10.1016/j.nucengdes.2014.01.032

[15] Brinkman, H.C. (1952) The Viscosity of Concentrated Suspensions and Solutions. *The Journal of Chemical Physics*, **20**, 571-571. https://doi.org/10.1063/1.1700493

[16] Abu-Nada, E. (2008) Application of Nanofluids for Heat Transfer Enhancement of Separated Flows Encountered in a Backward Facing Step. *International Journal of Heat and Fluid Flow*, **29**, 242-249. https://doi.org/10.1016/j.ijheatfluidflow.2007.07.001

[17] Cebeci, T. and Bradshaw, P. (1984) Physical and Computational Aspects of Convective Heat Transfer. Springer.

[18] Ahmed, S.E., Hussein, A.K., Mansour, M.A., Raizah, Z.A. and Zhang, X. (2018) MHD Mixed Convection in Trapezoidal Enclosures Filled with Micropolar Nanofluids. *Nanoscience and Technology: An International Journal*, **9**, 343-372. https://doi.org/10.1615/nanoscitechnolintj.2018026118

[19] Nachtsheim, P.R. and Swigert, P. (1965) Satisfaction of Asymptotic Boundary Conditions in Numerical Solution of Systems of Nonlinear Equations of Boundary-Layer Type. NASA TND 3004.

[20] Al-Shimmary, A.F.A. (2017) Solving Initial Value Problem using Runge-Kutta 6th Order Method. *ARPN Journal of Engineering and Applied Sciences*, **12**, 3953-3961.

[21] Blasius, H. (1908) Grenzschichten in Flussigkeiten Mit Kleiner Reibung. *Zeitschrift für angewandte Mathematik und Physik*, **56**, 1-37.

[22] Ishak, A., Nazar, R. and Pop, I. (2008) Flow and Heat Transfer Characteristics on a Moving Flat Plate in a Parallel Stream with Constant Surface Heat Flux. *Heat and Mass Transfer*, **45**, 563-567. https://doi.org/10.1007/s00231-008-0462-9